Neuron

Circuit Reorganization Shapes the Developing Human Foveal Midget Connectome toward Single-Cone Resolution

Highlights

- For best visual acuity, human foveal cones transmit via a non-divergent midget circuit
- Developing foveal midget circuits are shaped by extensive synaptic remodeling
- Foveal midget circuit refinement commences weeks before mid-gestation
- Cone photoreceptor-midget bipolar cell connectivity is adult-like before birth

Authors

Chi Zhang, Yeon Jin Kim, Ana R. Silverstein, Akina Hoshino, Thomas A. Reh, Dennis M. Dacey, Rachel O. Wong

Correspondence

dmd@uw.edu (D.M.D.), wongr2@uw.edu (R.O.W.)

In Brief

Zhang et al. carry out serial electron microscopy volume imaging in the human fovea. They show that the adult midget synaptic connectome is sculpted progressively by extensive circuit remodeling beginning in fetal life to produce a "private-line" circuit arrangement that is specialized for perceiving fine spatial detail.

Zhang et al., 2020, Neuron *108*, 1–14
December 9, 2020
https://doi.org/10.1016/j.neuron.2020.09.014

CellPress

Please cite this article in press as: Zhang et al., Circuit Reorganization Shapes the Developing Human Foveal Midget Connectome toward Single-Cone Resolution, Neuron (2020), https://doi.org/10.1016/j.neuron.2020.09.014

Neuron

CellPress

Article

Circuit Reorganization Shapes the Developing Human Foveal Midget Connectome toward Single-Cone Resolution

Chi Zhang,[1] Yeon Jin Kim,[1] Ana R. Silverstein,[1] Akina Hoshino,[1] Thomas A. Reh,[1] Dennis M. Dacey,[1,*] and Rachel O. Wong[1,2,*]

[1]Department of Biological Structure, University of Washington, Seattle, WA 98195, USA

[2]Lead Contact

*Correspondence: dmd@uw.edu (D.M.D.), wongr2@uw.edu (R.O.W.)

https://doi.org/10.1016/j.neuron.2020.09.014

SUMMARY

The human visual pathway is specialized for the perception of fine spatial detail. The neural circuitry that determines visual acuity begins in the retinal fovea, where the resolution afforded by a dense array of cone photoreceptors is preserved in the retinal output by a remarkable non-divergent circuit: cone → midget bipolar interneuron → midget ganglion cell (the "private line"). How the private line develops is unknown; it could involve early specification of extremely precise synaptic connections or, by contrast, emerge slowly in concordance with the gradual maturation of foveal architecture and visual sensitivity. To distinguish between these hypotheses, we reconstructed the midget circuitry in the fetal human fovea by serial electron microscopy. We discovered that the midget private line is sculpted by synaptic remodeling beginning early in fetal life, with midget bipolar cells contacting a single cone by mid-gestation and bipolar cell-ganglion cell connectivity undergoing a more protracted period of refinement.

INTRODUCTION

The retina of many vertebrates show a local region of elevated cell density serving high-acuity vision (Hughes, 1977). In primates, the high-acuity region is the fovea, a pit-like depression within which cone photoreceptors are densely packed and rod photoreceptors are largely absent (Curcio et al., 1990; Polyak, 1941; Zhang et al., 2015). Foveal cone photoreceptors extend long axons, the fibers of Henle, that connect with inner retinal neurons that are displaced away from the foveal center (Drasdo et al., 2007; Hendrickson et al., 2012; Polyak, 1941; Sjöstrand et al., 1999).

Cone photoreceptors in the foveal center are extremely small (~2 μm diameter) and densely packed and thus sample visual space optimally (Curcio et al., 1990; Merigan and Katz, 1990; Rossi and Roorda, 2010; Thibos et al., 1987; Williams, 1986). To preserve the exquisite spatial resolution afforded by the foveal cone array, a unique circuit, referred to as the midget pathway, has evolved. In the midget circuit, each cone photoreceptor synapses upon a single ON and OFF midget bipolar cell which in turn synapse exclusively or nearly exclusively upon single ON and OFF midget ganglion cells (Boycott and Dowling, 1969; Calkins et al., 1994; Kolb and Marshak, 2003; Polyak, 1941; Wool et al., 2019). ON cells are depolarized and OFF cells hyperpolarized by light onset (Famiglietti and Kolb, 1976; Kuffler, 1953). The lack of synaptic divergence and convergence in this "private-line" midget pathway contrasts sharply with other common retinal circuits, where many cones synapse on bipolar cells and many bipolar cells synapse upon single ganglion cells. The foveal midget circuit thus represents an extreme specialization with the goal of preserving spatial sampling by individual cones at the level of the midget ganglion cells to set the neural limit on human visual acuity (Hirsch and Curcio, 1989; Rossi and Roorda, 2010; Watson, 2014; Wilkinson et al., 2016). Despite its critical role in human vision, how the midget private line is established during development is unknown.

The development of the human fovea is a surprisingly protracted process that continues well after birth (Hendrickson et al., 2012; Hendrickson and Yuodelis, 1984). Previous studies suggest that there is an improvement in contrast sensitivity and visual acuity from newborns to early childhood (Candy et al., 1998; Dobson and Teller, 1978; Hansen et al., 2009). Changes in cone photoreceptor morphology and packing density likely underlie some of these improvements. Cones become thinner and increase their inner and outer segment lengths after birth (Hendrickson et al., 2012; Hendrickson and Yuodelis, 1984; Vajzovic et al., 2012). Also, cone packing density increases as cone photoreceptors migrate centripetally toward the foveal center (Candy et al., 1998; Curcio et al., 1990; Diaz-Araya and Provis, 1992). However, factors downstream of the photoreceptors are also required to fully account for the differences between immature and adult visual performance (Banks and Bennett, 1988; Brown, 1990; Candy and Banks, 1999; Candy et al., 1998; Wilson, 1988). One possibility is that the midget circuitry

Please cite this article in press as: Zhang et al., Circuit Reorganization Shapes the Developing Human Foveal Midget Connectome toward Single-Cone Resolution, Neuron (2020), https://doi.org/10.1016/j.neuron.2020.09.014

itself also undergoes developmental remodeling in order to acquire the unique private-line configuration.

The overall developmental progression of circuit assembly in the human fovea shares some similarities with other mammals. Neurogenesis, synaptogenesis, and cell death all occur before mid-gestation (Bumsted and Hendrickson, 1999; Cornish et al., 2004; Curcio et al., 1990; Diaz-Araya and Provis, 1992; Hendrickson and Zhang, 2019; Xiao and Hendrickson, 2000). All neuronal types differentiate in the incipient fovea by fetal week 10 in a sequence similar to that reported in mice, followed by synaptogenesis in the inner plexiform layer (IPL) and outer plexiform layer (OPL) at approximately fetal week 11 (Hendrickson and Zhang, 2019; Hendrickson, 1996; Hoshino et al., 2017; Linberg and Fisher, 1990; van Driel et al., 1990). During synaptogenesis, massive waves of naturally occurring death of foveal bipolar and ganglion cells occur, peaking at approximately fetal weeks 15 and 20 for these cell types, respectively, and reducing their numbers by half (Georges et al., 1999; Provis and van Driel, 1985). Further, as in rodents, OFF connections in the IPL precede that of the ON connections (Hendrickson, 1996).

However, the timeline of human foveal development also exhibits some distinctive features. Foveal bipolar cells differentiate weeks earlier than the peak of ganglion cell death (Georges et al., 1999; Hoshino et al., 2017), whereas in rodents (Morrow et al., 2008), rabbits (Wu and Chiao, 2007), ferrets (Miller et al., 1999), and cats (Maslim and Stone, 1986), bipolar cell genesis largely occurs after ganglion cell death (Sernagor et al., 2001). The sequence of synaptogenesis is also different in the primate fovea. In both human and monkey, bipolar cell ribbon synapses are generated more rapidly than the conventional synapses of amacrine cells, the reverse order of many other mammals (Hendrickson, 1996). Moreover, unlike in other species, large cell movements (the migration of cones into and displacement of ganglion cells away from the foveal center) occur and extend into the postnatal period (Diaz-Araya and Provis, 1992; Provis et al., 1985). These observations raise the possibility that the foveal midget private line may follow a progression of circuit maturation that varies from that adopted by other mammals.

To determine the developmental strategy responsible for establishing the midget private line, we used serial block-face scanning electron microscopy (SBEM) to reconstruct emerging circuitry in the developing human fovea when cones, bipolar cells, and ganglion cells were evident and synaptogenesis was underway. We identified cone and bipolar cell synaptic ribbons to evaluate midget circuitry up to approximately mid-gestation, when cells begin to be displaced from the center of the fovea. In addition, we have applied the same methods to reconstruct a small sample of foveal midget circuits in a single adult human retina in order to compare more quantitatively the morphology and synaptic arrangement of the adult private line with its developing counterpart.

RESULTS

Serial Block-Face Reconstructions of the Midget Private-Line Circuit in Adult Retina

The non-divergent synaptic connectivity of the midget pathway has been characterized in detail in the non-human primate (Calkins et al., 1994; Jusuf et al., 2006; Klug et al., 2003; Schein et al., 2011; Wool et al., 2019). For the human fovea, reconstructions derived from traditional transmission electron microscopy (TEM) methods are more limited (Kolb and Dekorver, 1991) and there is some evidence that the midget circuit may be more convergent, i.e., some midget ganglion cells receive synaptic input from more than one midget bipolar cell (Kolb and Marshak, 2003). Moreover, there is recent evidence that in the periphery of the macaque monkey retina midget ganglion cells receive significant synaptic input from non-midget ("diffuse") bipolar types and that midget bipolar cells can synapse with non-midget ganglion cell types (Tsukamoto and Omi, 2015, 2016). Thus, before considering the development of the midget circuit we needed to evaluate the basic morphological and synaptic features of this pathway in an adult human retina from our SBEM reconstructions.

We reconstructed adult midget circuitry from vertical sections and imaged an area ~500 μm from the foveal center (within the central 1° of the visual field) that extended from the cone synaptic pedicle in the OPL to the inner border of the ganglion cell layer. Cone pedicles at this central retinal location contained 20–27 synaptic ribbons (23 ± 2.5; mean ± SD, n = 12 cells). Midget bipolar cells showed a unique morphological relationship to cone synaptic ribbons that distinguishes them from all other bipolar cell types (see also Calkins, 1999; Tsukamoto and Omi, 2015, 2016). Consistent with previous light and electron microscopy studies, our SBEM reconstructions showed both ON and OFF midget bipolar cells extended single stout dendrites from the cell body to the pedicle base (Figures 1A and 1B). ON midget bipolar cells made distinctive invaginating contacts, closely approaching the ribbon synapse (Figures 1C and 1F). Each ribbon synapse was associated with a single invaginating terminal dendrite of an ON midget bipolar cell. The ON bipolar cell dendritic tip formed the central element in a synaptic triad that included the presynaptic ribbon and laterally placed horizontal cell processes (Figures 1D and 1E). By contrast, OFF midget bipolar cell terminals formed non-invaginating or basal (also referred to as flat) contacts with the pedicle synaptic face (Figures 1C and 1F). A key feature of both the adult ON and OFF midget bipolar cell is that their dendritic terminals converge upon and rarely extend beyond a single cone synaptic pedicle.

The midget bipolar → midget ganglion cell connection is also morphologically distinct (Calkins et al., 1994; Wool et al., 2019). We reconstructed the synaptic connectivity of four neighboring midget ganglion cell ON and OFF circuits; an example of one ON and OFF cell pair is illustrated in Figure 2. We found the ganglion cell dendritic tree—barely 5 μm in diameter—enveloped a single bulb-like bipolar cell synaptic terminal making a glomerular-like connection with the great majority of bipolar cell ribbon synapses directed to this single ganglion cell (Figures 2A–2C; Video S1). Midget bipolar cell ribbon densities showed little variability either within or across the ON and OFF bipolar samples (Figure 2D; unpaired t test, $p > 0.05$), and the overall morphology of this synapse appeared remarkably similar to that described in the macaque monkey using the same SBEM methods (Wool et al., 2019). ON and OFF midget bipolar cells targeted all or nearly all synaptic output to a single midget ganglion cell as anticipated; one ON and one OFF midget bipolar directed output

Please cite this article in press as: Zhang et al., Circuit Reorganization Shapes the Developing Human Foveal Midget Connectome toward Single-Cone Resolution, Neuron (2020), https://doi.org/10.1016/j.neuron.2020.09.014

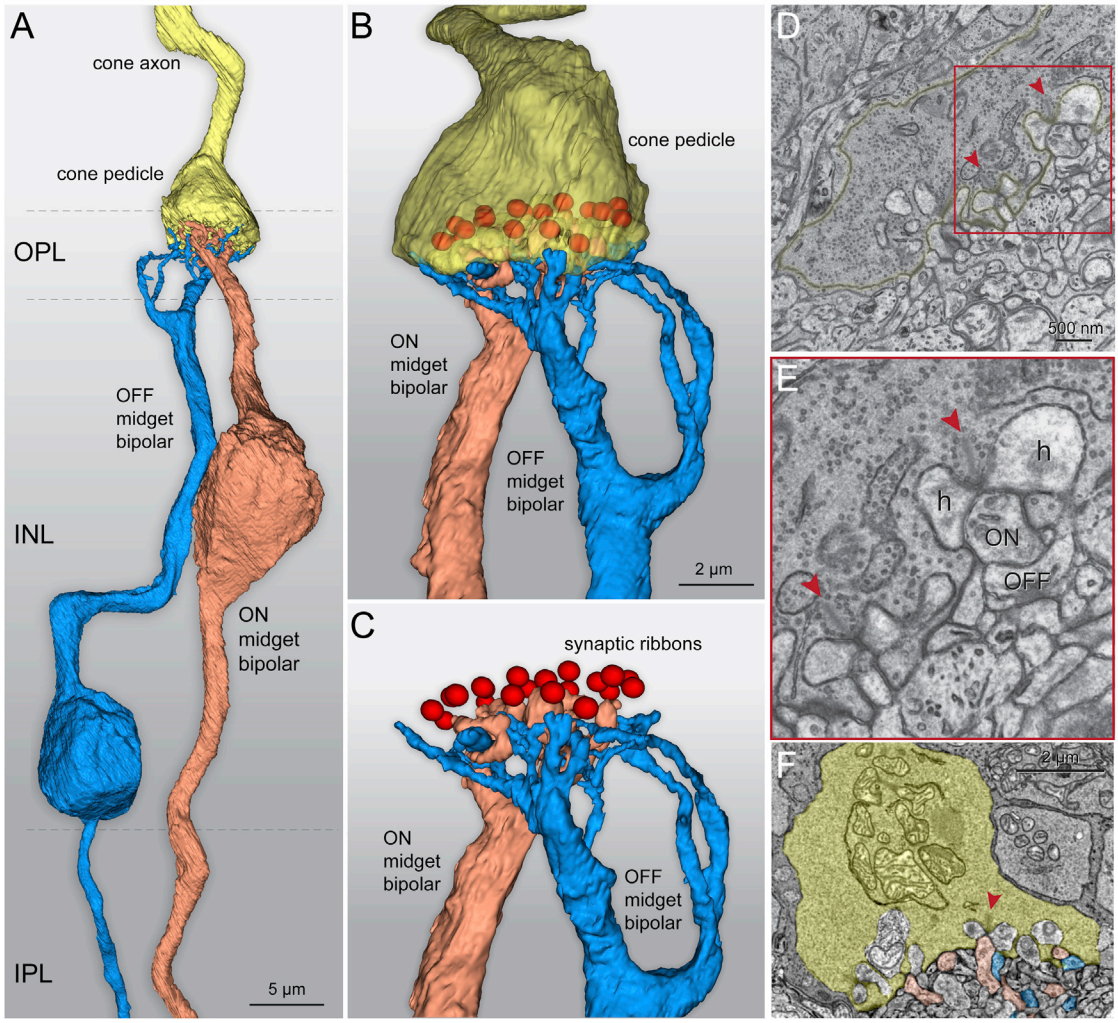

Figure 1. Morphology of the Private-Line Midget Circuit in the Adult Human Retina: the Cone → Bipolar Cell Synapse and Synaptic Triad

(A) SBEM-based reconstruction of a proximal cone axon and pedicle (yellow fill) and the ON and OFF midget bipolar cells (copper and blue fills) that contact this single cone (~500 µm from the foveal center). OPL, outer plexiform layer; INL, inner nuclear layer; IPL, inner plexiform layer.

(B) Zoomed-in view of pedicle in (A) rotated 180°. The pedicle is shown in partial transparency; each presynaptic ribbon location and size are indicated by the red balls at the pedicle base. The ON and OFF bipolar cells do not extend terminal dendritic processes laterally beyond the base of the pedicle.

(C) As in (B) but with the pedicle fully transparent to show the invaginating ON bipolar terminals close to the ribbons relative to the basal OFF midget bipolar terminals at the pedicle base.

(D) High-resolution TEM image of another pedicle (outlined in yellow) illustrating two synaptic triads (red arrowheads) where invaginating ON and basal OFF bipolar cells appose each ribbon.

(E) Boxed area in (D) shown at higher zoom illustrates the ultrastructural components of the adult synaptic triad. Red arrowheads point to the presynaptic ribbons flanked by a halo of synaptic vesicles. The dendritic terminals of horizontal cell interneurons (h, lateral elements) on either side of the ON midget bipolar dendrite (ON, central element) create a distinctive butterfly pattern. OFF midget bipolar dendrites are associated with the invaginating ON bipolar dendrite (OFF, triad associated).

(F) SBEM volume illustrating one image layer of the cone pedicle (yellow shading) shown in (A)–(C). One synaptic triad is indicated by the red arrowhead with ON midget bipolar process (copper) and a basal OFF midget bipolar terminal (blue) at this triad.

to two neighboring midget ganglion cells (Figures 2E and 2F; Table S1). Conversely, two of four ON midget ganglion cells received significant input from a second midget bipolar cell, and one of four OFF midget ganglion cells received a minor secondary input (Table S2; Video S1). In addition to these small departures from the idealized private-line connection, all ON and OFF midget ganglion cells received a minor input from non-midget or diffuse bipolar types, and midget bipolar cells made a minor synaptic output to non-midget ganglion cell types, as evidenced by their large dendritic trees in our reconstructions (Tables S1 and S2).

ON and OFF Midget Bipolar Cells Form Input and Output Synapses before Mid-gestation

The location of the future foveal pit first appears early in the retina's developmental timeline (Figure 3A) as a retinal thickening that

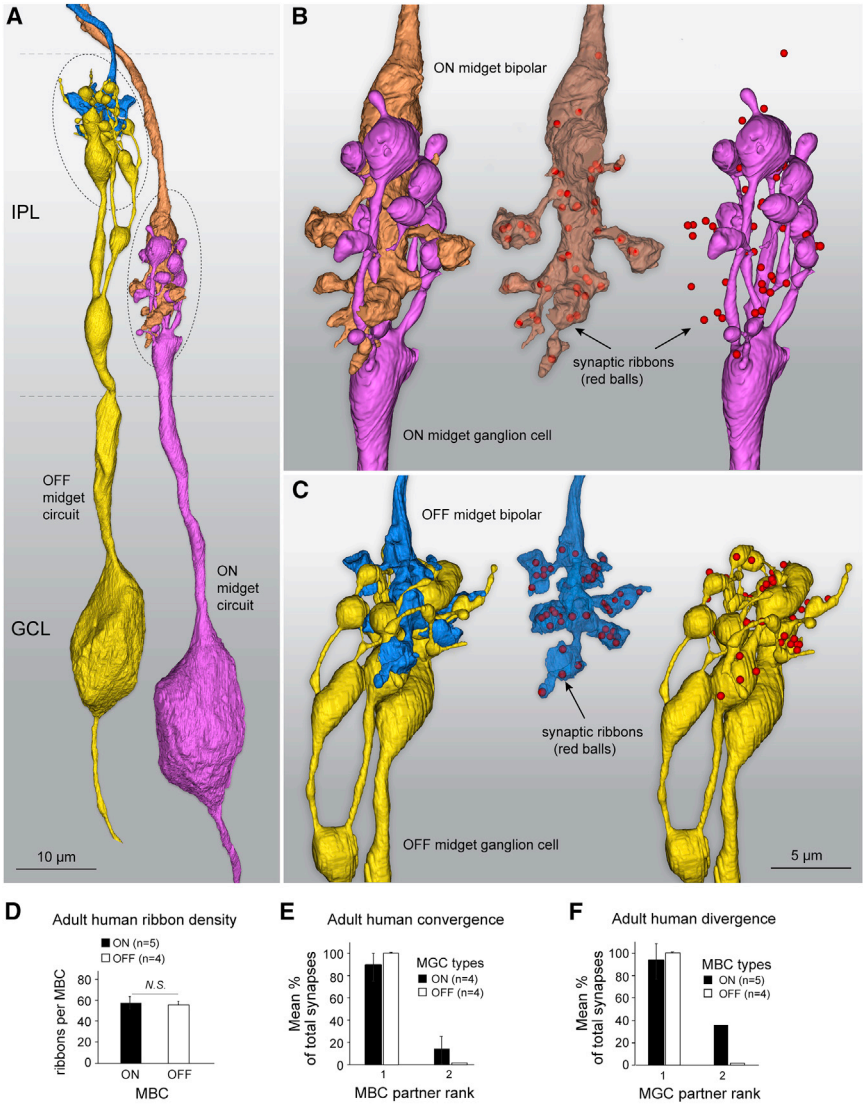

Figure 2. Morphology of the Private-Line Midget Circuit in the Adult Human Retina: the Inner Plexiform Layer (IPL)

(A) Single ON (copper) and OFF (blue) midget bipolar axon terminals forming spatially restricted synaptic connections (encircled regions) with single midget ganglion cells (violet and yellow fills). The ganglion cell dendrites converge upon and envelope the midget bipolar cells, creating a glomerular structure that is ~5 µm in diameter. GCL, ganglion cell layer.

(B) Left: zoomed-in view of the ON midget bipolar-ganglion cell connection shown in (A). Center: the ON bipolar cell is shown alone in semi-transparency, with red balls indicating the position and approximately size of synaptic ribbons within the terminal. Right: the midget ganglion cell dendritic tree shown in relation to the midget bipolar ribbons. 77% of the ribbons (37) synapse upon this ganglion cell; the remaining ribbons contact non-midget ganglion cells (7) or amacrine cell interneurons (4).

(C) Same format as (B) but for the OFF midget circuit shown in (A). Of the 52 synaptic ribbons, 47 (90%) contacted the midget ganglion cell and 4 contacted amacrine cells.

(D) The average number of ribbons of ON (n = 5) and OFF (n = 4) midget bipolar cells (unpaired t test).

(E and F) Quantification of private-line synaptic connectivity between ON and OFF midget bipolar and midget ganglion. (E) Midget circuit convergence plots the proportion of total synapses each midget ganglion cell receives from a midget bipolar cell (rank of 1 on the x axis denotes a bipolar cell providing the majority of synaptic input to a midget ganglion cell). (F) Divergence of midget bipolar cell synapses across midget ganglion cell partners. As in (E); rank 1 on the x axis denotes the dominant midget ganglion cell partner.

Data are shown as mean ± SD; n, number of cells; *N.S.*, no significant difference ($p > 0.05$).

See also Video S1.

forms a distinctive rounded dome in the temporal retina (Figure S1A). To characterize the development of the midget circuit, we first identified this incipient foveal region in isolated fetal human retinas (see STAR Methods). We prepared retinal pieces encompassing this developing foveal region for SBEM reconstructions across the entire depth of the retina (Figure S1; Video S2). All the cells reconstructed were within 250 µm from the center of the foveal dome, within which previous studies and our immunostaining (Figure S1B) revealed long (L)- and medium (M)-wavelength cones but a lack of short (S)-wavelength cones, features characteristic of the adult fovea (Cornish et al., 2004; Xiao and Hendrickson, 2000). We examined retinas between fetal weeks 14 and 21, during which synaptic ribbons are present in the OPL and IPL, as demonstrated by immunostaining with a ribbon marker (Figure 3B) (Hendrickson and Zhang, 2019; Hoshino et al., 2017).

Foveal cones between fetal weeks 14 and 21 showed immature morphology, with stubby outer segments, cuboidal cell bodies, and proto-pedicles extending numerous filopodia-like processes (Figure 3C). The diameter of the cone pedicles decreased with age, in parallel with an increase in cone packing over time (Diaz-Araya and Provis, 1992) (fetal week 14, 12.67 ± 0.86 µm; fetal week 18, 10.7 ± 30.99 µm; fetal week 21, 6.85 ± 1.06 µm; mean ± SD, n = 15, 20, and 13 cells, respectively; ordinary one-way ANOVA test, $p < 0.0001$). During this developmental period, bipolar cells with dendrites in the OPL and an axon terminal in the IPL could also be readily identified (Figure S1D). Bipolar cells with varying dendritic and axonal sizes were found; one population with relatively small dendritic and axonal arbors (both <200 µm^2) appeared numerically dominant, and even at fetal week 14, these cells were distinguishable from other bipolar cells that showed larger (>200 µm^2) dendritic and/or axonal arbors (Figure S1D). We refer to these small cells as midget bipolar cells (Figures 3D and S1D). Midget bipolar cells could also be distinguished as ON and OFF types as early as fetal week 14 by axonal stratification depth in the IPL (Figures 3D and S1D) (Boycott and Wässle, 1991; Tsukamoto and Omi, 2016).

Please cite this article in press as: Zhang et al., Circuit Reorganization Shapes the Developing Human Foveal Midget Connectome toward Single-Cone Resolution, Neuron (2020), https://doi.org/10.1016/j.neuron.2020.09.014

CellPress

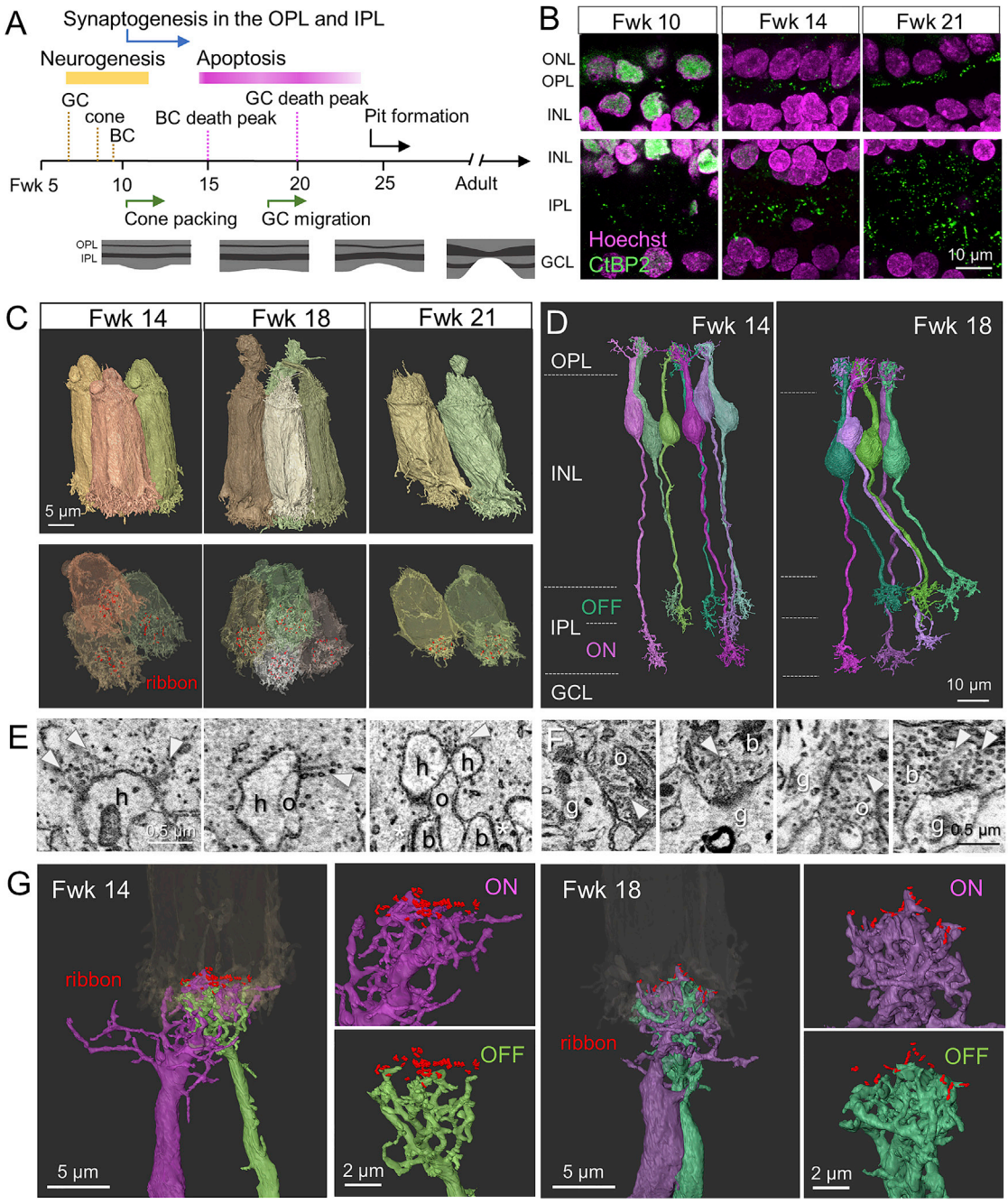

Figure 3. Synaptogenesis Involving ON and OFF Midget Bipolar Cells Occurs Prior to Mid-gestation

(A) Key developmental events of the human fovea with age (Georges et al., 1999; Hendrickson et al., 2012; Hendrickson and Zhang, 2019; Hendrickson, 1996; Hoshino et al., 2017; Provis et al., 2013). The foveal pit begins to form at approximately mid-gestation. Fwk, fetal week; OPL, outer plexiform layer; IPL, inner plexiform layer; BC, bipolar cell; GC, ganglion cell.

(B) Ribbon synapses within the OPL (top row) and IPL (bottom row) across fetal ages, immunolabeled by CtBP2 antibody. The nuclear layers are labeled by Hoechst staining. ONL, outer nuclear layer; INL, inner nuclear layer; GCL, ganglion cell layer.

(C) Morphology of fully reconstructed fetal foveal cones. Top: side views of cones. Bottom: rotated views of cone terminals with synaptic ribbons marked.

(D) Morphology of fetal foveal midget bipolar cells.

(E) Scanning electron microscopy images of ribbons (arrowheads) within cone terminals showing invaginating synapses with horizontal cells (h) and ON midget bipolar cells (o), and basal synaptic contacts (asterisks) with OFF midget bipolar cells (b). Left to right panels: fetal weeks 14, 18, and 21.

(legend continued on next page)

Please cite this article in press as: Zhang et al., Circuit Reorganization Shapes the Developing Human Foveal Midget Connectome toward Single-Cone Resolution, Neuron (2020), https://doi.org/10.1016/j.neuron.2020.09.014

As expected, synaptic ribbons were abundant in cones and bipolar cells between fetal weeks 14 and 21. Moreover horizontal cells and bipolar cells were postsynaptic to cones (Figure 3E), and ganglion cells were postsynaptic to bipolar cells (Figure 3F). We then asked whether, as in the adult (Figure 1), ON and OFF midget bipolar cells had already made their characteristic invaginating and basal synaptic contacts at cone pedicles at these fetal ages (Calkins et al., 1994; Dowling and Boycott, 1966; Hopkins and Boycott, 1997; Schein et al., 2011). We found evidence for both types of synaptic arrangements between fetal midget bipolar cells and cones at fetal weeks 14–21 (Figures 3E, 3G, S1E, and S1F; Video S2; see STAR Methods for more detailed criteria for defining OFF bipolar-cone synapses).

The Cone to Midget Bipolar Private Connection Is Adult-like by Mid-gestation

Midget bipolar cells in the adult retina form spatially restricted, compact dendritic arbors that converge upon and terminate at the synaptic face of a single cone pedicle (Figure 1) (Boycott and Wässle, 1991; Calkins et al., 1994; Kolb and Dekorver, 1991; Kolb and Marshak, 2003; Milam et al., 1993; Wässle et al., 1994; Wool et al., 2019). At fetal week 14, the pattern of cone to midget bipolar connectivity was similar, but not identical, to the adult pattern. Some ON (n = 5, 31% of 16 cells) and most OFF (n = 9, 82% of 11 cells) midget bipolar cells had a single highly branched but compact dendritic arbor that made dense membrane-to-membrane appositions with a single cone pedicle. Other ON (n = 5, 31%) and OFF (n = 1, 9%) cells principally contacted a single cone while also sparsely extended side branches to contact neighboring cones (Figures 4A and 4B). We also found some ON (n = 5, 31%) or OFF (n = 1, 9%) midget bipolar cells with more diffusely branched dendritic arbors compared to neighboring midget bipolar cells that extended across several cones (Figures 4B–4D). Occasionally, ON and OFF midget bipolar cell dendritic terminals were evenly divided between two cones (double arrows in Figure 4B). At fetal week 18, refinement of midget bipolar cell dendrites occurred as more ON (n = 8, 42% of 19 cells) and OFF (n = 16, 94% of 17 cells) cells restricted dendritic contacts to a single cone pedicle (Figures 4A and 4B).

To determine whether developmental progression in the incidence of contacts is paralleled by alterations in actual synaptic connectivity, we quantified synaptic convergence and divergence between cones and midget bipolar cells from fetal week 14 (see STAR Methods; Figures 5A–5C). Some midget bipolar cells clearly made synapses with more than one cone at fetal week 14 (Figure 5A). However, not all dendritic branches that contacted neighboring pedicles were associated with synaptic ribbons (Figures 4A and 5A). We also found an example of a midget bipolar cell that stratified in the ON portion of the IPL but had dendrites that contacted the cone pedicle without making invaginating synapses (Figures 4C and 4D). These more diffuse extensions of developing midget bipolar cells, while contrasting with that of the adult (Figure 1), may have made synapses earlier and were retracting, in the process of synaptogenesis, or simply failed to form a synapse.

Synaptic convergence and divergence between cones and the ON and OFF midget bipolar cells continued to refine with age (Figures 5A–5C). All ON and OFF midget bipolar cells reached a 1:1 synaptic connectivity with cones by between fetal weeks 18 and 21 (Figures 5B and 5C). At the same time, the ribbon synapse density of cones decreased to approximate the adult number between fetal weeks 14 and 21 (Figures 1 and 5D). Thus, by mid-gestation (fetal week 21), after a period of synaptic refinement, foveal cones and midget bipolar cells have attained the one-to-one connectivity and synaptic densities found in the mature retina. Furthermore, ON midget bipolar cells appear to lag behind OFF midget bipolar cells somewhat in the refinement of their dendritic morphology and connectivity.

In the adult cone synaptic triad, the ribbon is situated in a cleft apposing the invaginating ON cone bipolar dendritic terminal (Figure 1D–1F). The invaginating process is flanked by two larger, lateral elements that arise from horizontal cell interneurons. Finally, the invaginating process is encircled at the pedicle base by triad-associated basal contacts that arise from OFF midget bipolar cell dendrites (Tsukamoto and Omi, 2015). We found an increasing proportion of synapses with all these postsynaptic partner types between fetal weeks 14 and 21 (Figures 3E and 5E).

Presumed Midget Ganglion Cells Can Be Distinguished from Other Ganglion Cell Types Early in Development

Similar to the adult (Figure 2), developing presumed midget ganglion cells could be distinguished from all other ganglion cells by their small and compact dendritic trees. We reconstructed ganglion cells and their connectivity at fetal weeks 14 and 18, but nonoptimal ultrastructure prevented analysis of the inner retina for our fetal week 21 sample. At both fetal weeks 14 and 18, ganglion cells with either narrow, bushy dendritic trees or relatively wide, sparsely branching dendritic trees were found (Figures 6A–6D). The dendritic areas of the narrow-field ganglion cells and wide-field ganglion cells were significantly different (Figure 6A). Occasionally, we encountered displaced narrow-field ganglion cells with somata in the inner nuclear layer (Figure 6D) that synapsed with midget bipolar cells. Finally, as expected for midget circuits, the majority of ganglion cells contacted by identified midget bipolar cells were narrow-field ganglion cells (Figure 6E). Thus, we considered all narrow-field ganglion cells that synapsed with the midget bipolar cells, including the displaced cells, as midget ganglion cells for further analysis.

At fetal week 14, when most midget bipolar cells already have axons strongly biased to either the ON or OFF sublamina, the dendritic stratification levels of many midget ganglion cells are not yet well defined (Figures 6B and 7A). Midget ganglion cells

(F) Scanning electron microscopy images of ribbon synapses (arrowheads) in the IPL showing ON (o) and OFF (b) midget bipolar cells axons contacting ganglion cells (g). Left two panels: fetal week 14. Right two panels: fetal week 18.

(G) Representative pairs of ON and OFF midget bipolar cell dendritic arbors synapsing with the same cone at fetal weeks 14 and 18. All the ribbons in the contacted cones are indicated to show their spatial locations relative to these ON and OFF midget bipolar cell dendritic tips.

See also Figure S1 and Video S2.

Please cite this article in press as: Zhang et al., Circuit Reorganization Shapes the Developing Human Foveal Midget Connectome toward Single-Cone Resolution, Neuron (2020), https://doi.org/10.1016/j.neuron.2020.09.014

CellPress

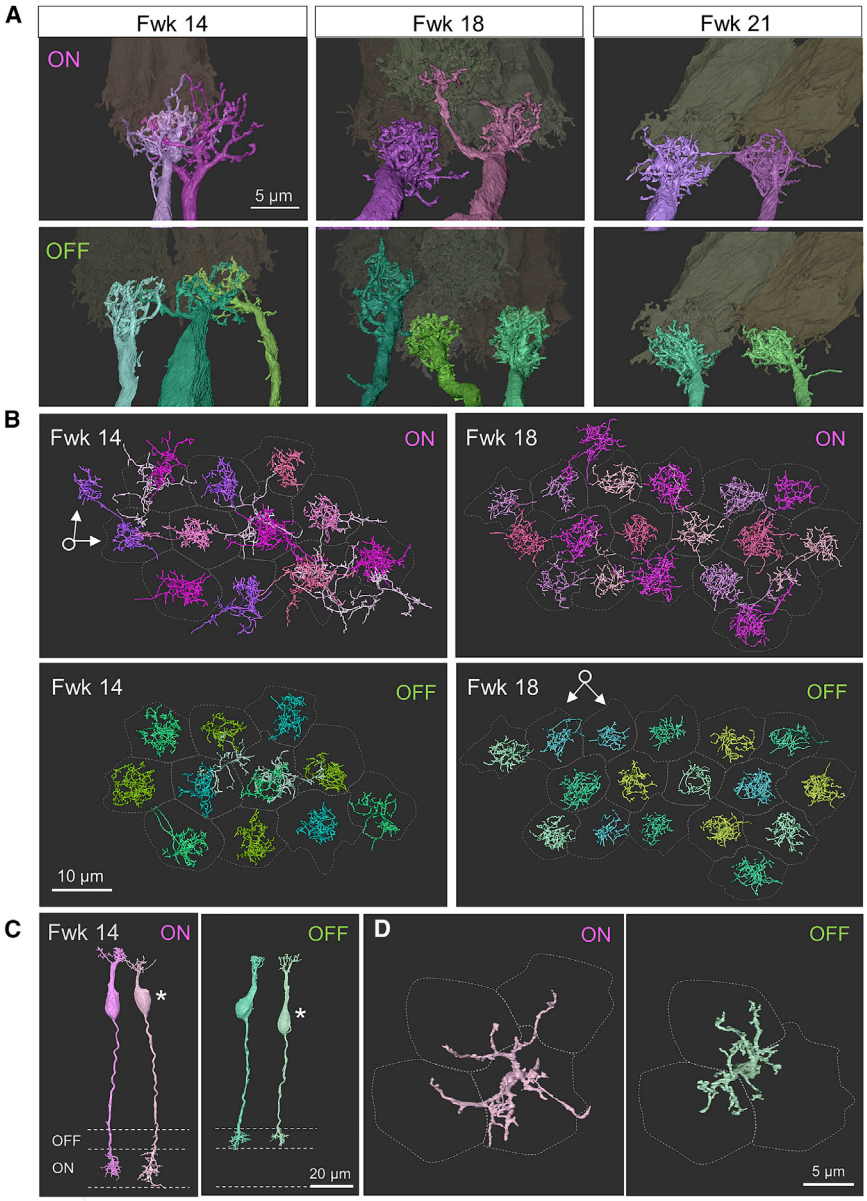

Figure 4. Foveal Midget Bipolar Cell Dendritic Contact Is Not Necessarily Restricted to a Single Cone before Mid-gestation

(A) Examples of ON (top) and OFF (bottom) midget bipolar cell dendritic arbors and their cone partners.

(B) Mosaics of ON and OFF midget bipolar cell dendritic arbors (skeletonized) that contact 11 cones (outlined by gray dashed lines) at fetal week 14 and 17 cones at fetal week 18. One fetal week 14 ON midget bipolar cell show and one fetal week 18 OFF midget bipolar cell show an evenly bifurcated dendritic arbor, as indicated by the double arrows. Dendritic arbors that appear relatively more diffuse (light pink and light green) belong to bipolar cells that were classified as midget bipolar cells based on their axonal morphology (see bipolar cells indicated with asterisks in C).

(C) Morphology of fetal week 14 ON and OFF midget bipolar cells, which have compact dendritic arbors, (magenta and green) and neighboring midget bipolar cells, which have more diffuse dendritic arbors (light pink and light green, indicated with asterisks). These bipolar cells all have midget axon terminals.

(D) *En face* views of the dendritic arbors of the ON and OFF midget bipolar cells indicated with asterisks in (C). The cone pedicles that are contacted by these cells are outlined by gray dashed contours. The ON midget bipolar cell did not synapse with the cones its dendrites touched.

with dendritic arbors that are confined within the ON sublamina were observed more frequently than those with an OFF-only stratifying arbor (Figures 6B and 7A). The separation of ON and OFF midget ganglion cell dendritic arbors became more evident by fetal week 18 (Figures 6C and 7B). Thus, although retinal ganglion cells are born and differentiated weeks earlier than bipolar cells (Hendrickson, 2016; Hoshino et al., 2017) (Figure 3A), bipolar cell axonal stratification appears to precede dendritic lamination of many, and especially OFF, midget ganglion cells.

Connectivity between Midget Bipolar Cells and Midget Ganglion Cells Undergoes Significant Remodeling with Maturation

When we mapped the ribbon synapses between midget bipolar and ganglion cells, we found dramatic changes in the specific relationships between these synaptic partners. At fetal week 14, when many of the midget ganglion cells dendrites were not strictly confined to the ON or OFF sublaminae, both ON and OFF midget bipolar cell made convergent synaptic contact with these dendrites (Figures 7C and 8A). When dendritic arbors became better stratified at fetal week 18 (Figure 7E), a given midget ganglion cell synapsed exclusively with either ON or OFF midget bipolar cells. This was the case even in instances where a few dendrites traversed across both ON and OFF sublaminae. Also, at fetal week 14, ganglion cells synapsing with either ON or OFF midget bipolar cells were contacted by more than one midget bipolar cell (Figure 7C). The degree of convergence to ON and OFF midget ganglion cells did not decrease between fetal weeks 14 and 18 (Figure 8B). However, the proportion of synapses between an ON midget ganglion cell and its primary midget bipolar cell partner, the partner that made the most synapses with the ganglion cell, increased during this period (Figures 7C, 7E, 8D, and 8E; unpaired t test, $p = 0.018$), approaching the biased configuration observed for the adult retina (Figure 2). OFF midget ganglion cells also showed a similar increase in the proportion of synapses with the primary bipolar cell partners, but these changes were not statistically significant (Figures 7C, 7E, 8D, and 8E; Mann-Whitney test, $p = 0.47$). Total ribbon synapse numbers of ON midget bipolar cells

Please cite this article in press as: Zhang et al., Circuit Reorganization Shapes the Developing Human Foveal Midget Connectome toward Single-Cone Resolution, Neuron (2020), https://doi.org/10.1016/j.neuron.2020.09.014

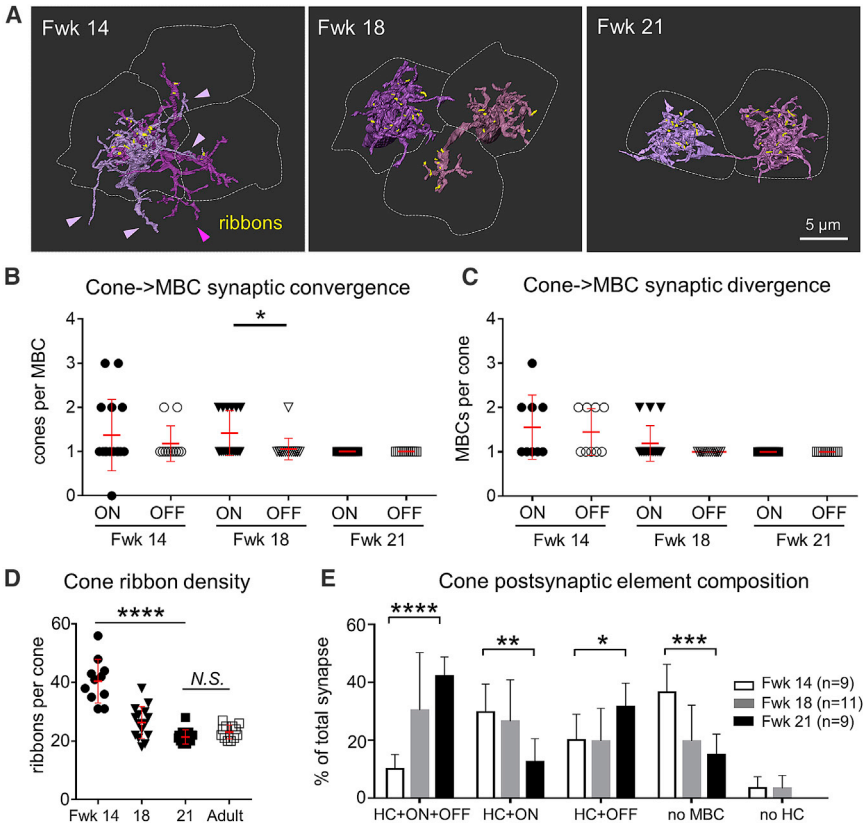

Figure 5. Foveal Cone and Midget Bipolar Cell Synaptic Connectivity Undergoes Refinement during Development

(A) *En face* views of dendritic arbors of the same ON midget bipolar cells in Figure 2A at fetal weeks 14, 18, and 21. The cone terminals innervated by the midget bipolar cells are outlined by gray dashed lines. Cone ribbons apposed to the bipolar cells shown are labeled in yellow. The side branches of fetal week 14 midget bipolar cells that touch but do not make ribbon synapses with cones are indicated by arrowheads in the same color as the associated bipolar cell.

(B) Cone to midget bipolar cell (MBC) synaptic convergence shown here by the number of cones synapsing with individual midget bipolar cells across ages (fetal week 14: ON, n = 16 midget bipolar cells; OFF, n = 11; fetal week 18: ON, n = 19; OFF, n = 17; fetal week 21: ON, n = 11; OFF, n = 11; n, number of cells; Mann-Whitney test).

(C) Cone to midget bipolar cell synaptic divergence is represented by the number of midget bipolar cells synapsing with an individual cone. Shown here is the divergence across ages (fetal week 14, n = 9 cones; fetal week 18, n = 16; fetal week 21, n = 11; Mann-Whitney test).

(D) Cone ribbon density across ages (fetal week 14, n = 11 cones; fetal week 18, n = 15; fetal week 21, n = 13; adult, n = 12; fetal weeks 14–21 comparison, Kruskal-Wallis test; fetal week 21 versus adult, Mann-Whitney test).

(E) The mean percentage of cone ribbons that were associated with different combinations of postsynaptic partners across ages (ordinary one-way ANOVA test). n, number of cones. Data are shown as mean ± SD.

*p < 0.05; **p < 0.01; ***p < 0.001; ****p < 0.0001. *N.S.*, no significant difference (p > 0.05).

decreased significantly between fetal weeks 14 and 18 (Figure 8F), suggesting that synapse elimination was involved in the refinement in their connectivity with the ON midget ganglion cells.

At fetal week 14, synaptic divergence of midget bipolar cells onto midget ganglion cells also exceeded the one-to-one connectivity typical of the mature circuit. ON and OFF midget bipolar cells had on average >10 postsynaptic midget ganglion cell partners, with the dominant ganglion cell partner receiving up to 30% of the total synapses from an individual midget bipolar cell (Figures 7D, 8C, 8G, S2A, and S2B). As the development progressed, many fetal week 18 ON midget bipolar cells had a preferred midget ganglion cell partner that received >50% of that midget bipolar cell's synapses (Figures 7F, 8H, and S2C). In contrast, most fetal week 18 OFF midget bipolar cells still distributed their synapses to multiple midget ganglion cells, often with two or more midget ganglion cells together receiving >50% of the midget bipolar cell's synapses (Figures 7F, 8H, S2D, and S2E). Nonetheless, a rough private line is in place by fetal week 18, as the level of divergence significantly decreased for both ON and OFF midget ganglion cells (Figures 7F and 8C).

DISCUSSION

The picture of the midget circuit emerging in our reconstructions of adult fovea is broadly consistent with previous observations in both human (Kolb and Marshak, 2003) and macaque monkey (Calkins, 1999). Departures from the pure private line at the bipolar-ganglion cell connection noted here are perhaps not surprising given our results from the fetal retina revealing that the midget circuit arises by extensive remodeling of quite diffuse connectivity at this synapse.

The Foveal Midget Pathway Is Shaped by Extensive Circuit Refinement

The major cell types that comprise the human midget pathway (i.e., cones, midget bipolar cells, and midget ganglion cells) can be recognized morphologically in the fovea at fetal week 14. We found that cones initially synapse with more than one midget bipolar cell and vice versa, and midget ganglion cells demonstrate a large degree of synaptic convergence and divergence with midget bipolar cells. By fetal week 18, midget bipolar cells receive all or nearly all of their photoreceptor input from a single cone and in turn direct the majority of their synaptic output to single midget ganglion cells. Cell death occurring in both the bipolar cell and ganglion cell populations between fetal weeks 14 and 18 likely contributes to refinement of the midget circuitry. However, our reconstructions underscored that the private line, while not perfect in the adult, arises through extensive synaptic remodeling. The decreases in cone and bipolar cell ribbon densities with age suggest that synapse elimination plays a role in

Please cite this article in press as: Zhang et al., Circuit Reorganization Shapes the Developing Human Foveal Midget Connectome toward Single-Cone Resolution, Neuron (2020), https://doi.org/10.1016/j.neuron.2020.09.014

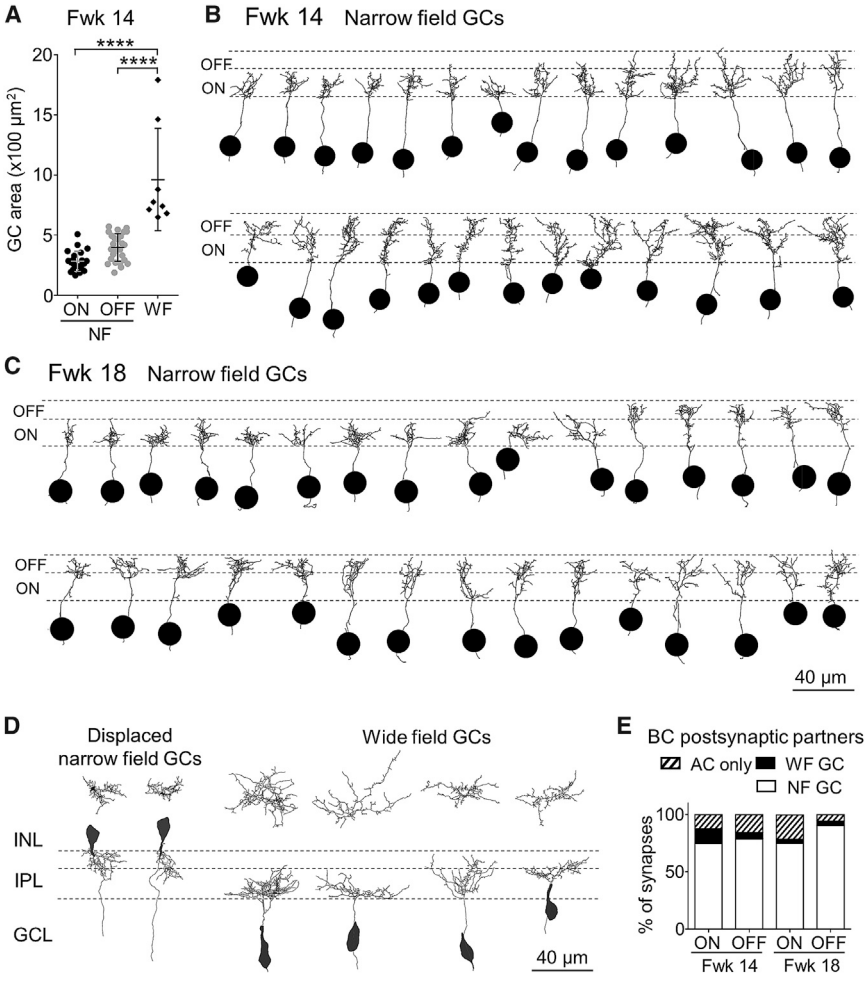

Figure 6. Dendritic Morphology and Stratification of Fetal Foveal Midget Ganglion Cells Remodel with Maturation

(A) Dendritic area sizes of narrow-field (NF) and wide-field (WF) ganglion cells at fetal week14 (ON narrow field, n = 22 midget ganglion cells [MGCs]; OFF narrow field, n = 26; wide field, n = 8; unpaired t test).

(B and C) Morphology of narrow-field ganglion cells at fetal weeks 14 and 18, with black disks indicating their somal position in the ganglion cell layer.

(D) Morphology of displaced narrow-field ganglion cells and wide-field ganglion cells at fetal week 14.

(E) Average proportions of the total number of synapses of midget bipolar cells that were attributed to narrow-field ganglion cells, wide-field ganglion cells, and amacrine cells (ACs) at fetal week 14 (ON, n = 7 midget bipolar cells; OFF, n = 5) and fetal week 18 (ON, n = 8; OFF, n = 8). "AC only" indicates that amacrine cell is the only cell type found at the particular midget bipolar cell ribbon synapse.

Data are shown as mean ± SD. ****p < 0.0001. n, number of cells.

the remodeling process. Although synaptic remodeling is a common feature of developing circuits across species (D'Orazi et al., 2014; Kast and Levitt, 2019; Okawa et al., 2014; Riccomagno and Kolodkin, 2015), we were somewhat surprised by the extent of remodeling, particularly between midget bipolar cells and midget ganglion cells, which seems more elaborate mechanistically than necessary to construct circuits with minimal cell diversity and simple connectivity and comprises repeated "units."

Narrow-field ganglion cells, the presumed midget cells, were the predominant ganglion cell type in the developing fovea. We cannot rule out that narrow-field ganglion cells elaborate a larger dendritic arbor later in development or that the wide-field ganglion cells undergo dendritic pruning and attain a more compact arbor. If these scenarios occur, then synaptic divergence from midget bipolar cells would be even greater with each midget bipolar cell presynaptic to higher numbers of either non-midget or midget ganglion cells than we estimated.

Differential Rates of Maturation along the Foveal Midget Pathway

We found that connectivity of the ON and the OFF midget bipolar cells is refined more rapidly with cone photoreceptors than with midget ganglion cells. This order of refinement is unlikely due to earlier synaptogenesis of midget bipolar cells with cones than with midget ganglion cells, because in the fovea, ribbon synapses are detected earlier in the IPL than in the OPL (Hendrickson, 1996). Several factors may contribute to the relatively faster synaptic refinement in the OPL. First, physical disassembly of synapses may progress more rapidly for cones compared to midget bipolar cells. Second, ganglion cells continue to die after midget bipolar cells and cones are stable and reach a one-to-one connectivity at approximately mid-gestation (Georges et al., 1999; Provis and van Driel, 1985). Finally, not all midget ganglion cell dendritic arbors have reached their adult stratification by fetal week 18, although midget bipolar cell axons are clearly stratified before this age.

Some aspects of the maturation sequence of the human foveal midget pathway contrast with previous observations in other species. In mouse, rat, rabbit, and ferret, retinal ganglion cell death is mostly complete prior to the peak of bipolar cell neurogenesis (Miller et al., 1999; Morrow et al., 2008; Sernagor et al., 2001; Wu and Chiao, 2007). Thus, unlike in the human fovea, bipolar cells in other species integrate into the retinal circuitry after ganglion cell numbers are finalized. Also, in mice, synaptogenesis between bipolar cells and ganglion cells commences at approximately postnatal day 7, after ON/OFF segregation of ganglion cell dendritic arbors is largely established (Coombs et al., 2007; Diao et al., 2004; Morgan et al., 2008; Sernagor et al., 2001). In contrast, midget bipolar cells in human fovea already synapse with midget ganglion cells before the dendritic arbors of many midget ganglion cells are well stratified. Furthermore, an anterograde sequence of

Please cite this article in press as: Zhang et al., Circuit Reorganization Shapes the Developing Human Foveal Midget Connectome toward Single-Cone Resolution, Neuron (2020), https://doi.org/10.1016/j.neuron.2020.09.014

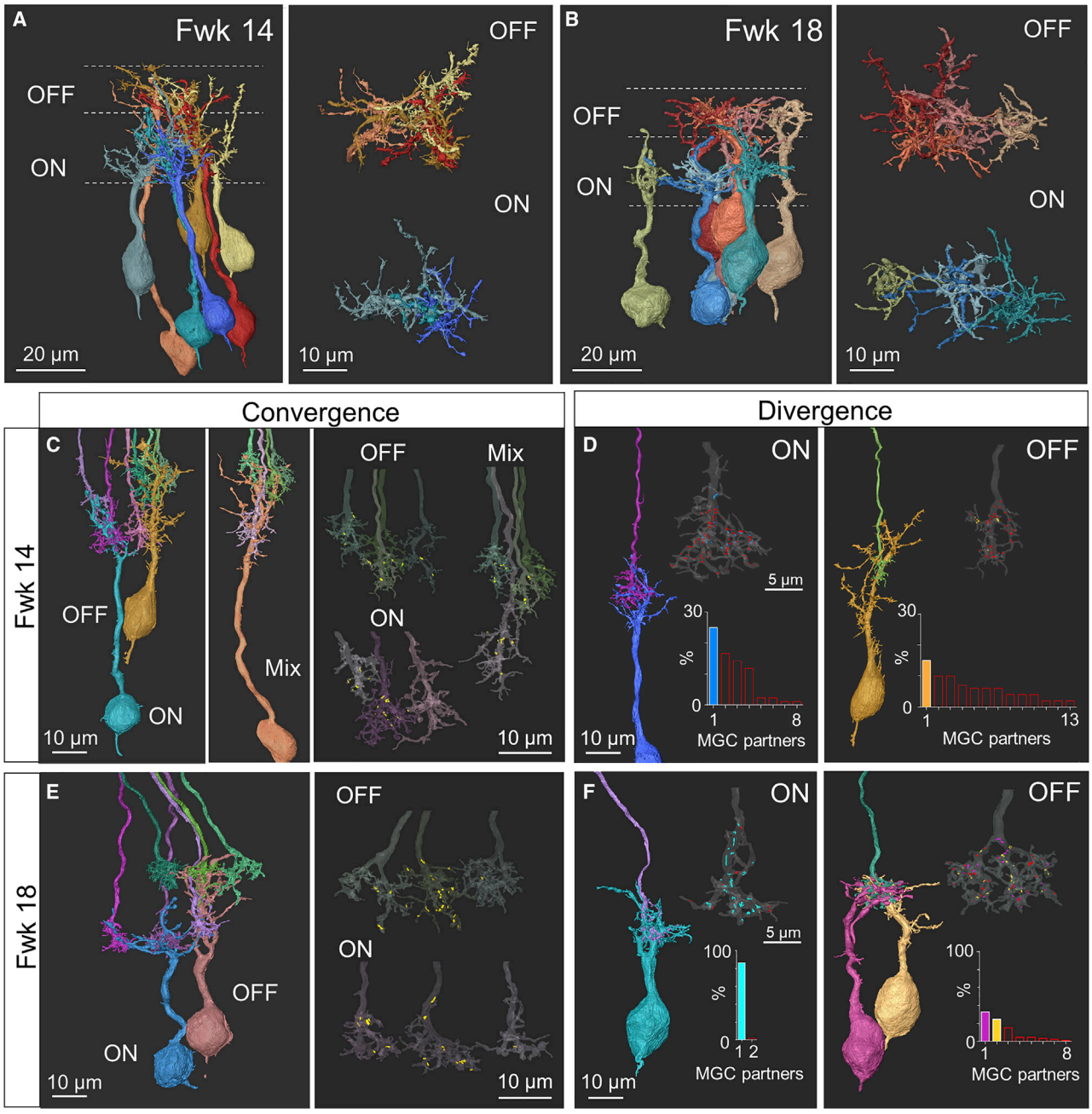

Figure 7. Synaptic Convergence and Divergence of Foveal Midget Bipolar Cells and Ganglion Cells Are Exuberant during Development

(A) ON and OFF midget ganglion cells at fetal week 14. Left: side view; right: *en face* view.

(B) ON and OFF midget ganglion cells at fetal week 18. Left: side view; right: *en face* view.

(C and E) Midget bipolar-ganglion cell synaptic convergence at fetal weeks 14 and 18. "Mix" indicates converging input from ON and OFF midget bipolar cells. For each midget ganglion cell, their postsynaptic densities are marked in yellow over the translucent outline of their midget bipolar cell partners (right panels) to show the location of the synapses.

(D and F) Representative midget bipolar cell axons and their dominant midget ganglion cell partner(s) at fetal weeks 14 and 18. The ribbons associated with the dominant midget ganglion cell(s) are marked in the corresponding color in the top right corner, whereas the remaining ribbons that belong to minor ganglion cell partners are in red. The histograms in each panel show the distribution of synaptic contacts across all the midget ganglion cell partners, with the filled bars representing dominant partner(s) with corresponding color and hollow bars outlined in red representing the minor partners. %, percentage of the total number of synapses of the midget ganglion cell shown in each panel.

See also Figure S2.

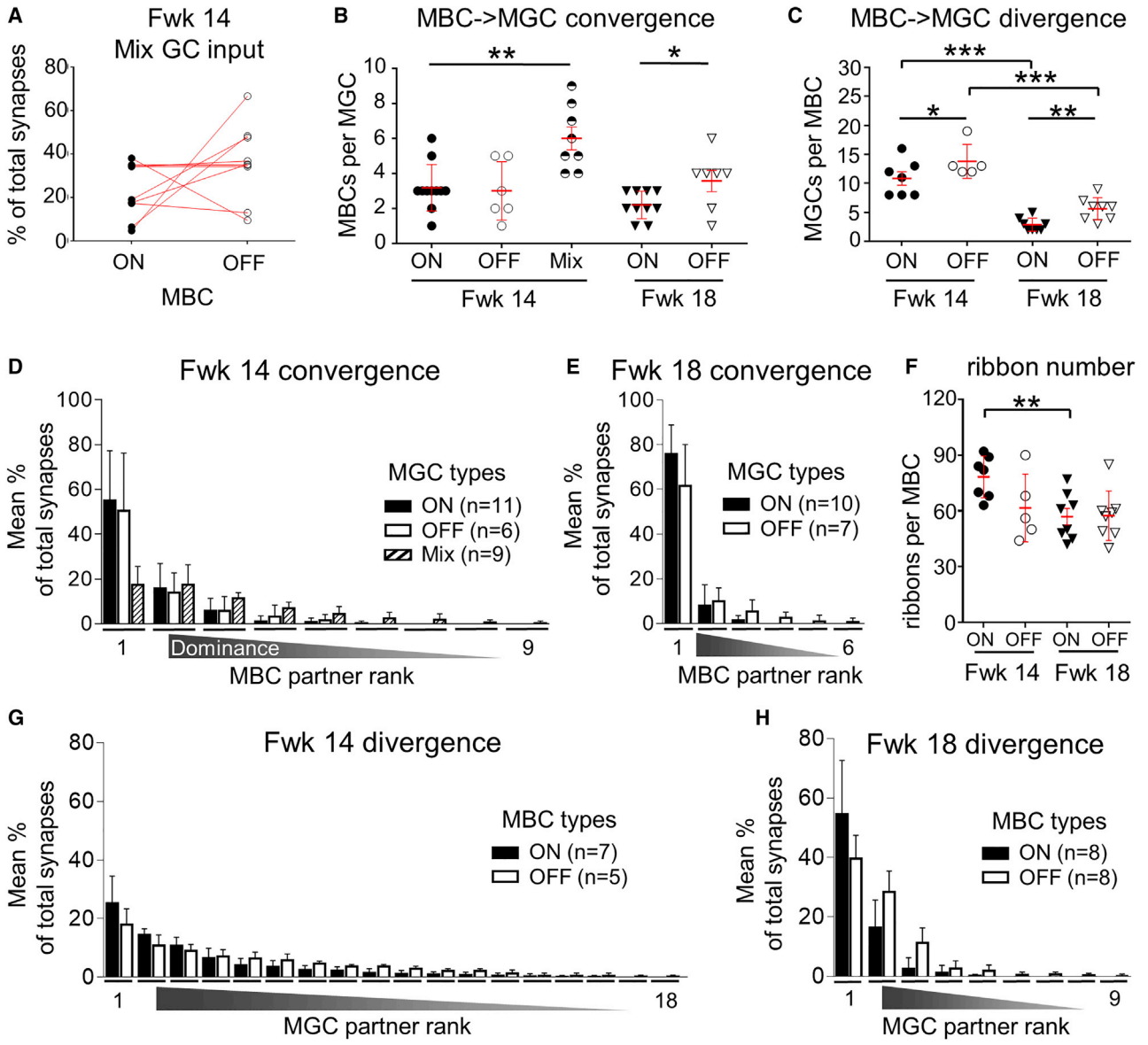

Figure 8. Quantification of the Synaptic Connectivity of Developing Foveal Midget Ganglion Cells

(A) Percentage of ON versus OFF midget bipolar cell (MBC) synapses formed with each midget ganglion cell (GC) that receives both input types at fetal week 14. Data points connected by red lines belong to the same cell.

(B) Midget bipolar-ganglion cell synaptic convergence represented by the number of midget bipolar cell synaptic partners of individual midget ganglion cells (MGCs) at fetal week 14 (ON, n = 11; OFF, n = 6; mix, ON and OFF, n = 9; Kruskal-Wallis test) and fetal week 18 (ON, n = 10; OFF, n = 7; Mann-Whitney test).

(C) Midget bipolar-ganglion cell synaptic divergence represented by the number of midget ganglion cell synaptic partners of individual midget bipolar cells at fetal week 14 (ON, n = 7; OFF, n = 5; Mann-Whitney test) and fetal week 18 (ON, n = 8; OFF, n = 8; unpaired t test).

(D and E) The x axis plots the ranking of midget bipolar cell synaptic partners, where 1 represents the midget bipolar cell that provides the majority of the synapses onto the midget ganglion cell. The y axis charts the proportion of the total number of synapses each midget ganglion cell receives from the midget bipolar cell of each rank. For example, at fetal week 14, of the sampled midget ganglion cell populations, ~50% of the total number of synapses on ON and OFF midget ganglion cells are provided by the dominant midget bipolar cell partner (rank 1).

(F) Ribbon numbers of midget bipolar cell axons at fetal weeks 14 and 18 (fetal week 14 ON, n = 7 midget bipolar cells; OFF, n = 8; fetal week 18 ON, n = 5; OFF, n = 8; Mann-Whitney test).

(G and H) The distribution of midget bipolar cell ribbon synapses across their postsynaptic midget ganglion cell partners at fetal weeks 14 and 18. As in (E) and (F), 1 on the x axis denotes the dominant midget ganglion cell partner (i.e., the midget ganglion cell that received the most synapses from the midget bipolar cell). Data are shown as mean ± SD. N, number of cells. *p < 0.05; **p < 0.01; ***p < 0.001.

synapse maturation proceeds from retina to central targets in human. Retinogeniculate synaptogenesis occurs 3–4 weeks after retinal synaptogenesis (Khan et al., 1994), and eye-specific segregation of ganglion cell axons in the lateral geniculate nucleus (LGN) is observed at approximately mid-gestation, followed by the lamination of LGN neurons 2 weeks later (Hevner, 2000). The rapid synaptogenesis between cones and bipolar cells, and bipolar cells and ganglion cells in the fetal fovea may be advantageous. It ensures that the future private line is largely in place (by mid-gestation) before large-scale cell displacements and axonal and dendritic extensions occur as the foveal pit emerges (Diaz-Araya and Provis, 1992; Provis et al., 1985). Moreover, the foveal cone mosaic is likely established very early in development because of the lack of cone death (Georges et al., 1999; Provis and van Driel, 1985). Thus, if the midget bipolar cells synapse with cones and midget ganglion cells before the ganglion cell axons have largely connected with central targets, which occurs in rodents (Cang et al., 2018; Dunn and Wong, 2012; Morgan et al., 2011), foveal midget cells may only need to refine and elongate their already connected neurites to maintain the topographic representation of visual space set by the cone mosaic.

We also found differences in the maturation rates of the ON and OFF foveal midget pathways. The dendritic arbors and axonal stratification of OFF midget bipolar cells reach more mature configurations earlier than those of ON midget bipolar cells. In contrast, ON midget ganglion cells stratify earlier than OFF midget ganglion cells. In monkey retina, such differences between ON and OFF midget ganglion cells are less obvious (Kirby and Steineke, 1991). The human foveal private-line arrangement between cones and midget bipolar cells is also achieved earlier in the OFF pathway. Moreover, previous studies show that in the IPL of both human and monkey retinas, synaptogenesis occurs first in the OFF sublayer and then in the ON sublayer (Crooks et al., 1995; Okada et al., 1994; van Driel et al., 1990). We might thus expect that OFF midget bipolar-ganglion cell synaptic refinement also proceeds more quickly compared to the ON pathway. However, the OFF midget bipolar-ganglion cell connectivity refines more slowly compared to the ON connections. Thus, differences in the ON and OFF midget pathways are not necessarily pathway specific but instead are influenced by the differential maturation rates of their respective synaptic partner populations. For instance, the period of cell death of foveal OFF midget ganglion cells may be more protracted than that of ON midget ganglion cells, although this remains to be examined.

When Is the Foveal Private Line Fully Established?

Although connectivity along the cone-midget bipolar-midget ganglion cell pathways has undergone significant remodeling prior to fetal week 20, an excess of midget ganglion cells remained at this age, and the adult connectivity pattern has not yet been attained. Because foveal ganglion cell death peaks at approximately fetal week 20 and significantly decreases by fetal week 25 (Georges et al., 1999), and because ribbon synapse density in the human fovea reaches the adult level by mid-gestation, it is possible that the adult connectivity pattern emerges before pit formation. Alternatively, the refinement of the inner retinal midget circuitry may be as protracted as the large-scale structural and functional maturation of the fovea itself. Psychophysical and modeling studies indicate that human newborns have significantly poorer contrast sensitivity and visual acuity compared to adults (Dobson and Teller, 1978; Hansen et al., 2009) that cannot be fully explained by immaturities of the eye's optics and the cone photoreceptors (Banks and Bennett, 1988; Brown, 1990; Candy and Banks, 1999; Candy et al., 1998; Wilson, 1988). Therefore, refinement of midget circuits may be finalized gradually, possibly extending postnatally. If so, then improvement in visual resolution after birth may be due to the final refinement of the inner retinal circuitry as light-driven neural activity commences.

STAR★METHODS

Detailed methods are provided in the online version of this paper and include the following:

- KEY RESOURCES TABLE
- RESOURCE AVAILABILITY
  - Lead Contact
  - Materials Availability
  - Data and Code Availability
- EXPERIMENTAL MODEL AND SUBJECT DETAILS
  - Human tissue
- METHOD DETAILS
  - Identification of the foveal center
  - EM sample preparation and image acquisition
  - Volume reconstruction and analysis
  - Immunohistochemistry
  - Confocal image acquisition and processing
- QUANTIFICATION AND STATISTICAL ANALYSIS

SUPPLEMENTAL INFORMATION

Supplemental Information can be found online at https://doi.org/10.1016/j.neuron.2020.09.014.

ACKNOWLEDGMENTS

This work was supported by an Allen Distinguished Investigator award to T.A. Reh and R.O. Wong and NIH grants EY-06678 and EY-028282 to D.M. Dacey, 5R24 HD000836 (to I.A. Glass, the Birth Defects Research Lab), and EY-01730 (M. Neitz; Vision Core). We thank Ed Parker, Dale Cunningham, Sharm Knecht, and Orin Packer for technical assistance with electron microscopy and image volume preparation and Mike Marsh for help with 3D rendering using Dragonfly (Object Research Systems, Montreal, Canada). We thank Kaori Oda and Mike Ahlquist for assistance with electron microscopy image segmentation.

AUTHOR CONTRIBUTIONS

Conceptualization, C.Z., D.M.D., and R.O.W.; Methodology and Investigation, C.Z., Y.J.K., A.H., and D.M.D.; Data Analysis and Curation, C.Z., A.R.S., Y.J.K., and D.M.D.; Writing – Original Draft, C.Z., Y.J.K., D.M.D., and R.O.W.; Writing – Review & Editing, C.Z., Y.J.K., A.H., T.A.R., D.M.D., and R.O.W.

DECLARATION OF INTERESTS

The authors declare no competing interests.

Received: December 9, 2019
Revised: August 11, 2020
Accepted: September 8, 2020
Published: October 6, 2020

REFERENCES

Banks, M.S., and Bennett, P.J. (1988). Optical and photoreceptor immaturities limit the spatial and chromatic vision of human neonates. J. Opt. Soc. Am. A *5*, 2059–2079.

Boycott, B.B., and Dowling, J.E. (1969). Organization of the primate retina: light microscopy. Proc. R. Soc. Lond. B Biol. Sci. *255*, 109–176.

Boycott, B.B., and Wässle, H. (1991). Morphological classification of bipolar cells of the primate retina. Eur. J. Neurosci. *3*, 1069–1088.

Brown, A.M. (1990). Development of visual sensitivity to light and color vision in human infants: a critical review. Vision Res. *30*, 1159–1188.

Bumsted, K., and Hendrickson, A. (1999). Distribution and development of short-wavelength cones differ between Macaca monkey and human fovea. J. Comp. Neurol. *403*, 502–516.

Calkins, D.J. (1999). Synaptic organization of cone pathways in the primate retina. In Color Vision: From Genes to Perception, K.R. Gegenfurtner and L.T. Sharpe, eds. (Cambridge University Press), pp. 163–180.

Calkins, D.J., Schein, S.J., Tsukamoto, Y., and Sterling, P. (1994). M and L cones in macaque fovea connect to midget ganglion cells by different numbers of excitatory synapses. Nature *371*, 70–72.

Candy, T.R., and Banks, M.S. (1999). Use of an early nonlinearity to measure optical and receptor resolution in the human infant. Vision Res. *39*, 3386–3398.

Candy, T.R., Crowell, J.A., and Banks, M.S. (1998). Optical, receptoral, and retinal constraints on foveal and peripheral vision in the human neonate. Vision Res. *38*, 3857–3870.

Cang, J., Savier, E., Barchini, J., and Liu, X. (2018). Visual function, organization, and development of the mouse superior colliculus. Annu. Rev. Vis. Sci. *4*, 239–262.

Cardona, A., Saalfeld, S., Schindelin, J., Arganda-Carreras, I., Preibisch, S., Longair, M., Tomancak, P., Hartenstein, V., and Douglas, R.J. (2012). TrakEM2 software for neural circuit reconstruction. PLoS ONE *7*, e38011.

Coombs, J.L., Van Der List, D., and Chalupa, L.M. (2007). Morphological properties of mouse retinal ganglion cells during postnatal development. J. Comp. Neurol. *503*, 803–814.

Cornish, E.E., Hendrickson, A.E., and Provis, J.M. (2004). Distribution of short-wavelength-sensitive cones in human fetal and postnatal retina: early development of spatial order and density profiles. Vision Res. *44*, 2019–2026.

Crooks, J., Okada, M., and Hendrickson, A.E. (1995). Quantitative analysis of synaptogenesis in the inner plexiform layer of macaque monkey fovea. J. Comp. Neurol. *360*, 349–362.

Curcio, C.A., Sloan, K.R., Kalina, R.E., and Hendrickson, A.E. (1990). Human photoreceptor topography. J. Comp. Neurol. *292*, 497–523.

D'Orazi, F.D., Suzuki, S.C., and Wong, R.O. (2014). Neuronal remodeling in retinal circuit assembly, disassembly, and reassembly. Trends Neurosci. *37*, 594–603.

Della Santina, L., Kuo, S.P., Yoshimatsu, T., Okawa, H., Suzuki, S.C., Hoon, M., Tsuboyama, K., Rieke, F., and Wong, R.O.L. (2016). Glutamatergic monopolar interneurons provide a novel pathway of excitation in the mouse retina. Curr. Biol. *26*, 2070–2077.

Diao, L., Sun, W., Deng, Q., and He, S. (2004). Development of the mouse retina: emerging morphological diversity of the ganglion cells. J. Neurobiol. *61*, 236–249.

Diaz-Araya, C., and Provis, J.M. (1992). Evidence of photoreceptor migration during early foveal development: a quantitative analysis of human fetal retinae. Vis. Neurosci. *8*, 505–514.

Dobson, V., and Teller, D.Y. (1978). Visual acuity in human infants: a review and comparison of behavioral and electrophysiological studies. Vision Res. *18*, 1469–1483.

Dowling, J.E., and Boycott, B.B. (1966). Organization of the primate retina: electron microscopy. Proc. R. Soc. Lond. B Biol. Sci. *166*, 80–111.

Drasdo, N., Millican, C.L., Katholi, C.R., and Curcio, C.A. (2007). The length of Henle fibers in the human retina and a model of ganglion receptive field density in the visual field. Vision Res. *47*, 2901–2911.

Dunn, F.A., and Wong, R.O.L. (2012). Diverse strategies engaged in establishing stereotypic wiring patterns among neurons sharing a common input at the visual system's first synapse. J. Neurosci. *32*, 10306–10317.

Famiglietti, E.V., Jr., and Kolb, H. (1976). Structural basis for ON-and OFF-center responses in retinal ganglion cells. Science *194*, 193–195.

FitzSimmons, J., Fantel, A., and Shepard, T.H. (1994). Growth parameters in mid-trimester fetal Turner syndrome. Early Hum. Dev. *38*, 121–129.

Georges, P., Madigan, M.C., and Provis, J.M. (1999). Apoptosis during development of the human retina: relationship to foveal development and retinal synaptogenesis. J. Comp. Neurol. *413*, 198–208.

Hansen, R.M., Moskowitz, A., and Fulton, A.B. (2009). Multifocal ERG responses in infants. Invest. Ophthalmol. Vis. Sci. *50*, 470–475.

Hendrickson, A.E. (1996). Synaptic development in macaque monkey retina and its implications for other developmental sequences. Perspect. Dev. Neurobiol. *3*, 195–201.

Hendrickson, A. (2016). Development of retinal layers in prenatal human retina. Am. J. Ophthalmol. *161*, 29–35.e21.

Hendrickson, A.E., and Yuodelis, C. (1984). The morphological development of the human fovea. Ophthalmology *91*, 603–612.

Hendrickson, A., and Zhang, C. (2019). Development of cone photoreceptors and their synapses in the human and monkey fovea. J. Comp. Neurol. *527*, 38–51.

Hendrickson, A., Possin, D., Vajzovic, L., and Toth, C.A. (2012). Histologic development of the human fovea from midgestation to maturity. Am. J. Ophthalmol. *154*, 767–778.e762.

Herr, S., Ngo, I.T., Huang, T.M., Klug, K., Sterling, P., and Schein, S. (2011). Cone synapses in macaque fovea: II. Dendrites of OFF midget bipolar cells exhibit Inner Densities similar to their Outer synaptic Densities in basal contacts with cone terminals. Visual Neuroscience *28*, 17–28.

Hevner, R.F. (2000). Development of connections in the human visual system during fetal mid-gestation: a DiI-tracing study. J. Neuropathol. Exp. Neurol. *59*, 385–392.

Hirsch, J., and Curcio, C.A. (1989). The spatial resolution capacity of human foveal retina. Vision Res. *29*, 1095–1101.

Hopkins, J.M., and Boycott, B.B. (1997). The cone synapses of cone bipolar cells of primate retina. J. Neurocytol. *26*, 313–325.

Hoshino, A., Ratnapriya, R., Brooks, M.J., Chaitankar, V., Wilken, M.S., Zhang, C., Starostik, M.R., Gieser, L., La Torre, A., Nishio, M., et al. (2017). Molecular anatomy of the developing human retina. Dev. Cell *43*, 763–779.e764.

Hughes, A. (1977). The Topography of Vision in Mammals of Contrasting Lifestyles: Comparative Optics and Retinal Organisation (Springer-Verlag).

Jusuf, P.R., Martin, P.R., and Grünert, U. (2006). Synaptic connectivity in the midget-parvocellular pathway of primate central retina. J. Comp. Neurol. *494*, 260–274.

Kast, R.J., and Levitt, P. (2019). Precision in the development of neocortical architecture: From progenitors to cortical networks. Prog. Neurobiol. *175*, 77–95.

Khan, A.A., Wadhwa, S., and Bijlani, V. (1994). Development of human lateral geniculate nucleus: an electron microscopic study. Int. J. Dev. Neurosci. *12*, 661–672.

Kirby, M.A., and Steineke, T.C. (1991). Early dendritic outgrowth of primate retinal ganglion cells. Vis. Neurosci. *7*, 513–530.

Klug, K., Herr, S., Ngo, I.T., Sterling, P., and Schein, S. (2003). Macaque retina contains an S-cone OFF midget pathway. J. Neurosci. *23*, 9881–9887.

Kolb, H., and Dekorver, L. (1991). Midget ganglion cells of the parafovea of the human retina: a study by electron microscopy and serial section reconstructions. J. Comp. Neurol. *303*, 617–636.

Kolb, H., and Marshak, D. (2003). The midget pathways of the primate retina. Doc. Ophthalmol. *106*, 67–81.

Kuffler, S.W. (1953). Discharge patterns and functional organization of mammalian retina. J. Neurophysiol. *16*, 37–68.

Linberg, K.A., and Fisher, S.K. (1990). A burst of differentiation in the outer posterior retina of the eleven-week human fetus: an ultrastructural study. Vis. Neurosci. *5*, 43–60.

Maslim, J., and Stone, J. (1986). Synaptogenesis in the retina of the cat. Brain Res. *373*, 35–48.

Merigan, W.H., and Katz, L.M. (1990). Spatial resolution across the macaque retina. Vision Res. *30*, 985–991.

Milam, A.H., Dacey, D.M., and Dizhoor, A.M. (1993). Recoverin immunoreactivity in mammalian cone bipolar cells. Vis. Neurosci. *10*, 1–12.

Miller, E.D., Tran, M.N., Wong, G.K., Oakley, D.M., and Wong, R.O. (1999). Morphological differentiation of bipolar cells in the ferret retina. Vis. Neurosci. *16*, 1133–1144.

Morgan, J.L., Schubert, T., and Wong, R.O. (2008). Developmental patterning of glutamatergic synapses onto retinal ganglion cells. Neural Dev. *3*, 8.

Morgan, J.L., Soto, F., Wong, R.O.L., and Kerschensteiner, D. (2011). Development of cell type-specific connectivity patterns of converging excitatory axons in the retina. Neuron *71*, 1014–1021.

Morrow, E.M., Chen, C.M., and Cepko, C.L. (2008). Temporal order of bipolar cell genesis in the neural retina. Neural Dev. *3*, 2.

Okada, M., Erickson, A., and Hendrickson, A. (1994). Light and electron microscopic analysis of synaptic development in Macaca monkey retina as detected by immunocytochemical labeling for the synaptic vesicle protein, SV2. J. Comp. Neurol. *339*, 535–558.

Okawa, H., Hoon, M., Yoshimatsu, T., Della Santina, L., and Wong, R.O.L. (2014). Illuminating the multifaceted roles of neurotransmission in shaping neuronal circuitry. Neuron *83*, 1303–1318.

Polyak, S.L. (1941). The Retina (University of Chicago Press).

Provis, J.M., Dubis, A.M., Maddess, T., and Carroll, J. (2013). Adaptation of the central retina for high acuity vision: cones, the fovea and the avascular zone. Progress in retinal and eye research *35*, 63–81.

Provis, J.M., and van Driel, D. (1985). Retinal development in humans: the roles of differential growth rates, cell migration and naturally occurring cell death. Aust. N. Z. J. Ophthalmol. *13*, 125–133.

Provis, J.M., van Driel, D., Billson, F.A., and Russell, P. (1985). Development of the human retina: patterns of cell distribution and redistribution in the ganglion cell layer. J. Comp. Neurol. *233*, 429–451.

Riccomagno, M.M., and Kolodkin, A.L. (2015). Sculpting neural circuits by axon and dendrite pruning. Annu. Rev. Cell Dev. Biol. *31*, 779–805.

Rossi, E.A., and Roorda, A. (2010). The relationship between visual resolution and cone spacing in the human fovea. Nat. Neurosci. *13*, 156–157.

Schein, S., Ngo, I.T., Huang, T.M., Klug, K., Sterling, P., and Herr, S. (2011). Cone synapses in macaque fovea: I. Two types of non-S cones are distinguished by numbers of contacts with OFF midget bipolar cells. Vis. Neurosci. *28*, 3–16.

Sernagor, E., Eglen, S.J., and Wong, R.O. (2001). Development of retinal ganglion cell structure and function. Prog. Retin. Eye Res. *20*, 139–174.

Sjöstrand, J., Popovic, Z., Conradi, N., and Marshall, J. (1999). Morphometric study of the displacement of retinal ganglion cells subserving cones within the human fovea. Graefes Arch. Clin. Exp. Ophthalmol. *237*, 1014–1023.

Thibos, L.N., Cheney, F.E., and Walsh, D.J. (1987). Retinal limits to the detection and resolution of gratings. J. Opt. Soc. Am. A *4*, 1524–1529.

Tsukamoto, Y., and Omi, N. (2015). OFF bipolar cells in macaque retina: type-specific connectivity in the outer and inner synaptic layers. Front. Neuroanat. *9*, 122.

Tsukamoto, Y., and Omi, N. (2016). ON bipolar cells in macaque retina: type-specific synaptic connectivity with special reference to OFF counterparts. Front. Neuroanat. *10*, 104.

Vajzovic, L., Hendrickson, A.E., O'Connell, R.V., Clark, L.A., Tran-Viet, D., Possin, D., Chiu, S.J., Farsiu, S., and Toth, C.A. (2012). Maturation of the human fovea: correlation of spectral-domain optical coherence tomography findings with histology. Am. J. Ophthalmol. *154*, 779–789.e772.

van Driel, D., Provis, J.M., and Billson, F.A. (1990). Early differentiation of ganglion, amacrine, bipolar, and Muller cells in the developing fovea of human retina. J. Comp. Neurol. *291*, 203–219.

Wässle, H., Grünert, U., Martin, P.R., and Boycott, B.B. (1994). Immunocytochemical characterization and spatial distribution of midget bipolar cells in the macaque monkey retina. Vision Res. *34*, 561–579.

Watson, A.B. (2014). A formula for human retinal ganglion cell receptive field density as a function of visual field location. J. Vis. *14*, 15.

Wilkinson, M.O., Anderson, R.S., Bradley, A., and Thibos, L.N. (2016). Neural bandwidth of veridical perception across the visual field. J. Vis. *16*, 1.

Williams, D.R. (1986). Seeing through the photoreceptor mosaic. Trends Neurosci. *9*, 193–198.

Wilson, H.R. (1988). Development of spatiotemporal mechanisms in infant vision. Vision Res. *28*, 611–628.

Wool, L.E., Packer, O.S., Zaidi, Q., and Dacey, D.M. (2019). Connectomic identification and three-dimensional color tuning of S-OFF midget ganglion cells in the primate retina. J. Neurosci. *39*, 7893–7909.

Wu, M.L., and Chiao, C.C. (2007). Light deprivation delays morphological differentiation of bipolar cells in the rabbit retina. Brain Res. *1170*, 13–19.

Xiao, M., and Hendrickson, A. (2000). Spatial and temporal expression of short, long/medium, or both opsins in human fetal cones. J. Comp. Neurol. *425*, 545–559.

Zhang, T., Godara, P., Blanco, E.R., Griffin, R.L., Wang, X., Curcio, C.A., and Zhang, Y. (2015). Variability in human cone topography assessed by adaptive optics scanning laser ophthalmoscopy. Am. J. Ophthalmol. *160*, 290–300.e291.

Zhang, C., Yu, W.Q., Hoshino, A., Huang, J., Rieke, F., Reh, T.A., and Wong, R.O.L. (2019). Development of ON and OFF cholinergic amacrine cells in the human fetal retina. J. Comp. Neurol. *527*, 174–186.

Please cite this article in press as: Zhang et al., Circuit Reorganization Shapes the Developing Human Foveal Midget Connectome toward Single-Cone Resolution, Neuron (2020), https://doi.org/10.1016/j.neuron.2020.09.014

STAR★METHODS

KEY RESOURCES TABLE

REAGENT or RESOURCE	SOURCE	IDENTIFIER
Antibodies		
Mouse monoclonal anti-CtBP2	BD Biosciences	Cat.# 612044; RRID:AB_399431
Goat polyclonal anti-S cone opsin (OPN1SW, N-20)	Santa Cruz Biotechnology	Cat.# sc-14363; RRID:AB_2158332
Mouse monoclonal anti-L/M cone opsin (A12)	J. Huang, University of Washington, Seattle, WA	N/A
Donkey polyclonal anti-mouse IgG (H+L) Alexa Fluor 647	Jackson ImmunoResearch	Cat.# 715-605-151; RRID: AB_2340863
Donkey polyclonal anti-mouse IgG (H+L) Alexa Fluor 555	Invitrogen	Cat.# A-31570; RRID:AB_2536180
Donkey polyclonal anti-goat IgG (H+L) Alexa Fluor 568	Invitrogen	Cat.# A-11057; RRID:AB_2534104
Chemicals, Peptides, and Recombinant Proteins		
Ames' medium	Sigma	Cat.# A1420
Hoechst 33342	Invitrogen	Cat.# H1399
Normal Donkey Serum	Jackson ImmunoResearch	Cat.# 017-000-121; RRID: AB_2337258
Vectashield	Vector Laboratories	Cat# H-1000; RRID: AB_2336789
Toluidine blue	Electron Microscopy Services	Cat# 22050
Software and Algorithms		
Fiji	NIH	https://fiji.sc/; RRID: SCR_002285
Amira	Thermo-Fisher Scientific	https://www.thermofisher.com/global/en/home/industrial/electron-microscopy/electron-microscopy-instruments-workflow-solutions/3d-visualization-analysis-software/amira-life-sciences-biomedical.html; RRID: SCR_014305
Imaris	Bitplane	https://imaris.oxinst.com; RRID: SCR_007370
Dragonfly	ORS Visual SI	http://www.theobjects.com/dragonfly/index.html; RRID: SCR_002509

RESOURCE AVAILABILITY

Lead Contact

Further information and requests for resources and reagents should be directed to and will be fulfilled by the Lead Contact, Rachel O.L. Wong (wongr2@uw.edu).

Materials Availability

This study did not generate new unique reagents.

Data and Code Availability

No new code or unpublished software were used in this study. The datasets are too large to deposit online. Requests for original images should be sent to the corresponding authors.

EXPERIMENTAL MODEL AND SUBJECT DETAILS

Human tissue

Fetal retina tissue (male and female) was obtained from the Birth Defects Research Laboratory at the University of Washington using an approved protocol (UW5R24HD000836). Tissues had no identifiers, and ultrasounds along with physical characteristics such as fetal foot length and crown-rump were used to estimate the age (FitzSimmons et al., 1994). Age groups included fetal week10 (Fetal day (Fd) 72; n = 1), fetal week 14 (Fd96 and 101; n = 2), fetal week15 (Fd108; n = 1), fetal week 17 (Fd122; n = 1), fetal week18 (Fd127; n = 1), fetal week 21 (Fd145-147; n = 2). n = number of retinas.

Please cite this article in press as: Zhang et al., Circuit Reorganization Shapes the Developing Human Foveal Midget Connectome toward Single-Cone Resolution, Neuron (2020), https://doi.org/10.1016/j.neuron.2020.09.014

For the adult tissue sample, retina from a brain-dead organ donor (21 year old male) was acquired at the time of death and organ procurement from a collaboration between Sight Life (an eye banking service) and Life Center Northwest (an organ donor service). After cornea removal, eyes were placed in oxygenated Ames medium and further processed for electron microscopy following the protocol described below for fetal tissues.

METHOD DETAILS

Identification of the foveal center

In fetal human retina from fetal week 14 onward, the foveal center can be identified in the temporal retina from the ganglion cell layer side, which appears to be a 'dimple' in the center of a dome-shaped region (Figure S1A). The 'dimple' and 'dome' become more evident in older tissues, as more ganglion cells migrate tangentially away from the foveal center. Immunohistochemistry using antibodies against cone opsins confirmed that the 'dimple' co-localized with the S cone-free and L/M cone-rich foveal center (Figure S1B). The dimple and dome were used to locate the foveal center in the retina for serial block-face electron microscopy (SBEM).

To prepare each retinal sample for SBEM, we identified the dome-shaped area in temporal retina under a dissection scope. We then cut out this region, acquired a low magnification image and measured the distance of each edge of the piece from the foveal center. This enabled us to keep track of positions within the piece relative to the edges of the retinal piece. The piece was processed for SBEM. From toluidine-blue (1%) stained semithin resin sections viewed under light microscopy prior to SBEM imaging, we determined the region of the developing fovea as a rod free zone (about 700 μm in diameter), and where cones appeared more tightly packed. The center of this region corresponded to the 'dimple' and was identified by a small region that was surrounded by a much thicker ganglion cell layer (i.e., a 'dip' in ganglion cell thickness). These light microscopy images enabled us to trim the resin block further, while still encompassing the foveal center. Locations under SBEM corresponding to the light microscopy images were identified. We randomly selected a region < 250 μm from the foveal center of the piece and reconstructed a mosaic of cones and all the midget bipolar cells connected to these cones (see Figure 4). We then traced the ganglion cell partners of the bipolar cells. We believe that this approach is free of observer bias.

EM sample preparation and image acquisition

Both fetal and adult retina were dissected from eyecups in Ames' solution (Sigma) bubbled with 95%O_2/5%CO_2. Retinal pieces containing the fovea were fixed with 4% glutaraldehyde in 0.1M sodium cacodylate buffer, pH7.3-7.4 for 30 minutes to 1 hour at room temperature. Subsequently, the samples were prepared for the SEM as described previously (Della Santina et al., 2016). All the retinas were sectioned along the vertical axis of the retina to obtain images of retinal cross-sections. For the fetal tissues all images were acquired within 250 μm from the nominal or incipient foveal center, defined as the locus where cones formed a single nuclear layer in the outer retina and rods were rarely observed (Figure S1C). For the adult retina, images were acquired at ~500 μm from the foveal center, at a point where the foveal slope diminishes and the ganglion cell layer achieves maximal thickness. Previous measurements of ganglion cell displacement indicate that ganglion cells at this eccentricity would be linked to cones within 100 microns of the foveal center (Drasdo et al., 2007), well within the central 1 degree of the visual field and the region of peak visual acuity. In this study, we obtained EM micrographs of all the retinal layers in the fovea from one fetal week 14 (Fd101) and one fetal week 18 (Fd127) human retina; and from the OPL to the INL in the fovea of one fetal week 21 (Fd145) human retina (the inner retina's ultrastructure was not as well preserved). fetal weeks 14 and 18 fovea were serial sectioned and imaged on a 3View SEM microscope (Zeiss) at a voxel size of 6 × 6 x 60 nm^3. The adult and fetal week 21 foveal samples were imaged on a VolumeScope SEM (Apreo, Thermo Fisher Scientific) at a voxel size of 5 × 5 x 50 nm^3.

Volume reconstruction and analysis

EM micrographs were aligned using TrakEM2 (Cardona et al., 2012) in Fiji (NIH). The processes and somata of cells were manually traced and segmented using the AreaTree function, and synapses were annotated using the AreaList function of TrakEM2. In the outer retina, horizontal cells can be distinguished from bipolar cells by the absence of vertical axons and their somal locations in the outermost layer of the INL. ON bipolar cell synapses with cones were determined by the presence of ON bipolar cell invaginating processes directly opposed to anchored cone ribbons (Figure 1E). OFF bipolar cell basal synaptic contacts with cones were determined by the presence of symmetric thickening between OFF bipolar cell and cone pedicle membranes, which were less than 0.8 μm from the nearest anchored cone ribbon (Herr et al., 2011) (Figures 1E, S1E, and S1F). In the inner retina, ganglion cells were identified by the presence of an axon, whereas amacrine cells were recognized by the presence of presynaptic vesicles in their processes. Bipolar cell ribbon synapses were determined by the presence of postsynaptic density at the ganglion cell or amacrine cell membrane apposed to bipolar cell ribbons. The visualization of volume reconstructions and measurements of cell sizes was performed in TrakEM2 or Amira (Thermo Fisher Scientific) and Fiji (NIH). For bipolar cells, z-projections of their axonal and dendritic arbors were captured using Amira. The axonal and dendritic areas (x-y territories) were defined by the area within a polygon connecting the outermost axonal or dendritic tips, and measured using Fiji. The dendritic areas of retinal ganglion cells were determined similarly (Fiji).

Immunohistochemistry

Retinal frozen sections (14-20 μm thick) and wholemount preparations for immunohistochemistry were obtained as previously described (Zhang et al., 2019). Primary antibody incubation was performed at 4°C, and the tissue was incubated overnight for frozen sections and 4-5 days for wholemount retinas. Primary antibodies include anti-CtBP2 (mouse, 1:500, BD Biosciences), S cone opsin (goat, 1:50, Santa Cruz), and L/M cone opsin (Zhang et al., 2019) (mouse, 1:10, custom made at the University of Washington). Secondary antibody incubation was performed overnight at 4°C or for 2 hours at room temperature. Secondary antibodies used were anti-isotypic Alexa Fluor conjugates (1:1000, Invitrogen or Jackson ImmunoResearch). Hoechst 33342 (1:5,000, Invitrogen) was used to stain nuclei to indicate retinal nuclear layers.

Confocal image acquisition and processing

Fluorescence images were acquired on a TCS LSP8 confocal microscope (Leica), using a 0.75 numerical aperture (NA) 20x oil, or a 1.4 NA 63x oil objective lens; or an FV1000 confocal microscope (Olympus), using a 0.8 NA 20x oil, or a 1.35 NA 60x oil objective lens. Images were acquired at a x-y resolution of 0.05–0.8 μm/pixel and z step of 0.3–1 μm. Adjustment of contrast, brightness and hue, maximum intensity projections and three-dimensional visualization of images were all performed using Imaris (Bitplane).

QUANTIFICATION AND STATISTICAL ANALYSIS

Statistical analyses were performed using Prism (GraphPad). Distributions of each parameter were tested for normality using the D'Agostino and Pearson omnibus test and appropriate parametric or non-parametric statistical analyses were then applied. Unpaired t test (parametric) or Mann-Whitney test (non-parametric) was performed to compare (1) parameters between ON and OFF groups within the same retina; and (2) parameters of ON or OFF groups between two ages. Ordinary one-way analysis of variance (ANOVA) test (parametric) or Kruskal-Wallis test (non-parametric) was performed to compare the same parameter across more than two groups. Statistical methods and parameters including the value and meaning of 'n', mean ± SD and statistical significance are provided in the text or figure legends. Significance was determined at $p < 0.05$.